Title

A New Mutation in FIG4 Causes a Severe Form of CMT4J Involving TRPV4 in the Pathogenic Cascade

Journal

Journal of Neuropathology & Experimental Neurology, 76(9)

ISSN

0022-3069

Authors

Gentil, Benoit J
O'Ferrall, Erin
Chalk, Colin
et al.

Publication Date

2017-09-01

DOI

10.1093/jnen/nlx062

Peer reviewed

J Neuropathol Exp Neurol
Vol. 76, No. 9, September 2017, pp. 789–799
doi: 10.1093/jnen/nlx062

ORIGINAL ARTICLE

A New Mutation in *FIG4* Causes a Severe Form of CMT4J Involving TRPV4 in the Pathogenic Cascade

Benoit J. Gentil, PhD, Erin O'Ferrall, MD, Colin Chalk, MD, Luis F. Santana, PhD, Heather D. Durham, PhD, and Rami Massie, MD

Abstract

Mutations in *FIG4*, coding for a phosphoinositol(3,5) bisphosphate 5′ phosphatase and involved in vesicular trafficking and fusion, have been shown causing a recessive form of Charcot–Marie–Tooth (CMT). We have identified a novel intronic mutation in the *FIG4* in a wheel-chair bound patient presenting with a severe form of CMT4J and provide a longitudinal study. Investigations indicated a demyelinating sensorimotor polyneuropathy with diffuse active denervation and severe axonal loss. Genetic testing revealed that the patient is heterozygous for 2 *FIG4* mutations, p.I41T and a T > G transversion at IVS17-10, the latter predicted to cause a splicing defect. FIG4 was severely diminished in patient's fibroblasts indicating loss-of-function. Consistent with FIG4's function in phosphoinositol homeostasis and vesicular trafficking, fibroblasts contained multiple large vacuoles and vesicular organelles were abnormally dispersed. FIG4 deficiency has implications for turnover of membrane proteins. The transient receptor cation channel, TRPV4, accumulated at the plasma membrane of patient's fibroblasts due to slow turnover. Knocking down Fig4 in murine cultured motor neurons resulted in vacuolation and cell death. Inhibiting TRPV4 activity significantly preserved viability, although not correcting vesicular trafficking. In conclusion, we demonstrate a new FIG4 intronic mutation and, importantly, a functional interaction between FIG4 and TRPV4.

Key Words: Charcot–Marie–Tooth disease, Endosomes, FIG4, Motor neurons, Phosphoinositol(3,5) biphosphate, TRPV4.

INTRODUCTION

More than 100 genes have been linked to Charcot–Marie–Tooth disease (CMT), the most common inherited sensorimotor polyneuropathy. CMT can be caused by dominant (CMT1 and CMT2), X-linked or recessive (CMT4) mutations in genes affecting Schwann cell or axonal homeostasis leading to demyelinating or axonal forms of CMT, respectively (1). Mutations in *FIG4*, encoding a phosphoinositol(3,5) bisphosphate 5′ phosphatase can present as CMT4J (OMIM 611228), a rare form of recessive CMT (CMT4J). *FIG4* mutations have been increasingly identified in CMT patient cohorts with the use of exome sequencing. Heterozygous mutations in CMT patients carrying a p.I41T mutant and a null allele are commonly described. Other point mutations are described producing mutant FIG4p.L17P and p.E302K. The other alleles produce truncated mutants and are considered as null alleles, p.R183X, p.F98fsX102, p.D348fsX359, p.G253fsX261, p.F254SfsX7, and p.F98fsX38 (2, 3). Mutations in *FIG4* also are linked to rare forms of fatal neurodegenerative diseases, that is, amyotrophic lateral sclerosis (ALS11, OMIM 612577) and polymicrogyria (BTOP, OMIM 612691). Complete *FIG4* inactivation gives rise to a rare autosomal-recessive disease called Yunis-Varon syndrome (OMIM 216340), characterized by structural brain abnormalities, developmental delay and strong bone deformities (4). In this paper, we report identification of a novel intronic mutation in *FIG4*, a T > G transversion at IVS17-10, in conjunction with a p.I41T point mutation on the other allele in a patient presenting with a severe form of CMT.

CMT patients affected by mutations in FIG4 show an early-onset severe phenotype characterized by clumsy gait during childhood and an accelerated progressive asymmetrical limb weakness during the teen or adult years, often resulting in severe paralysis. Muscle weakness involves both proximal and distal muscles (5). Patients have minimal sensory complains despite signs of denervation and the constellation of symptoms may resemble amyotrophic lateral sclerosis. In contrast to CMT1, in which conduction velocities are uniformly decreased, reflecting diffuse demyelination, in CMT4J conduction block, temporal dispersion and asymmetric slowing of nerve conduction velocity are seen, mimicking acquired demyelinating neuropathies. In addition to conduction velocity slowing, EMG shows evidence of denervation, indicating axonal loss or motor neuron degeneration. Onion bulbs are

From the Department of Neurology and Neurosurgery & Montreal Neurological Institute, McGill University, Quebec, Canada (BJG, EO, CC, HDD, RM); and Department of Physiology & Biophysics and Howard Hughes Medical Institute, Department of Pharmacology, University of Washington, Seattle, Washington (LFS)
Send correspondence to: Benoit J. Gentil, PhD, Department of Neurology and Neurosurgery, Montreal Neurological Institute, Room 649, 3801 University St., Montreal, QC H3A 2B4, Canada; E-mail: benoit.gentil@mcgill.ca
Financial support: This work was supported by grants from ARSACS Foundation and ALS Canada and Merck Sharp & Dohme Corp.
Conflict of interest: The authors have no duality or conflicts of interest to declare.
Supplementary Data: Supplementary Data can be found at http://www.jnen.oxfordjournals.org.

observed in nerve biopsies (3, 5). Thus, although CMT4J is generally classified as a "demyelinating" form of CMT, axonal loss and denervation point to both neuronal and Schwann cell involvement. In the rodent nervous system, FIG4 is abundant in myelinating cells and in neurons, particularly dorsal root ganglion sensory neurons and spinal motor neurons (6).

A common feature of FIG4 pathology in patient-derived skin fibroblasts or in mouse models is the formation of large, clear vacuoles, indicating an altered processing of endolysosomal vesicles (2, 5). Phosphoinositols, including phosphoinositol(3) phosphate (PI(3)P) and $PI(3,5)P_2$ are important regulators of endolysomal processing. PI(3)P is a membrane marker of early endosomes, whereas $PI(3,5)P_2$ coats late endosomes and multivesicular bodies. Their relative levels are regulated by the Fab1 complex, which includes the scaffolding protein Vac14, the phosphoinositol 5 kinase, PIKfyve, and the phosphoinositol(3,5) bisphosphate 5 phosphatase, FIG4. In addition to its phosphatase activity, FIG4 stabilizes the Fab1 complex and acts as a PIKfyve activator in a positive feedback loop on $PI(3,5)P_2$ production (7).

PI(3)P is required for membrane recruitment of several proteins involved in regulating vesicular transport and intracellular protein sorting. Maturation from early to late endosome and fusion with lysosomes is dependent on $PI(3,5)P_2$ (8). The endogenous ligand of $PI(3,5)P_2$ is the lysosomal Ca^{2+} channel TRPML1, activation of which induces calcium efflux from the lysosome and allows the fission of the organelle and retrograde progression of the vesicle (9). These multiple functions are disrupted by FIG4 deficiency. In this study, cultured skin fibroblasts derived from the patient with the compound heterozygous *FIG4* mutation exhibited substantial decrease in FIG4 expression, accumulation of large vacuoles, and altered distribution and transport of vesicular organelles.

Inositol phosphates also modulate the activity and internalization of another membrane cation channel, transient receptor potential cation channel subfamily V member 4 (TRPV4), mutations in which cause another form of CMT, CMT2C (10–12). Interestingly, CMT2C-causing TRPV4 mutants show hyperactivity of the channel and massive calcium influx as key features of the pathology (13). Therefore, we hypothesized that FIG4 deficiency could disrupt TRPV4 dynamics or activity and, as a consequence, contribute to pathogenesis of CMT4J. Indeed, TRPV4 distribution and trafficking were dysregulated in FIG4-deficient cultured motor neurons establishing a functional link between FIG4 and TRPV4, and a mechanistic connection between CMT4J and CMT2C.

MATERIALS AND METHODS

Patient Information and Clinical Presentation

The patient was followed for several years in our neuromuscular clinic at the Montreal Neurological Hospital. Currently 48-years-old, this gentleman was diagnosed clinically with CMT at 13 years of age after presenting with poor sport performance, clumsiness, and mild gait difficulties. *Pes cavus*, hammer toes, shortened heel tendons, and distal sensory deficits were noted at that time. Early motor development was normal. Family history was not significant for other familial cases of neuropathy. In his middle 20s, he developed progressive weakness and atrophy in the right upper limb without any sensory abnormalities, starting focally in the triceps and spreading to proximal and distal right upper limb muscles within 2 years. This continued to spread to the proximal left arm muscles leading to a bilateral flail arm phenotype. He subsequently developed right quadriceps weakness which evolved to quadriparesis. At present, he remains quadriparetic with sensory symptoms and signs of sensory loss to all modalities only present in his distal feet. Cranial nerve function remains intact.

Nerve conduction studies at age 36 and 43 are presented in the Table. A clear demyelinating neuropathy not only with slowed conduction velocity, but also conduction blocks and temporal dispersion, were noted, along with severe axonal loss. Sensory responses were absent in the legs and showed decreased amplitudes in the upper limbs. Two lumbar punctures showed mildly elevated CSF protein (0.66 and 0.58 mg/L) with normal cell counts. A sural nerve biopsy and a brachial plexus biopsy were unrevealing. At that time an acquired demyelinating neuropathy was suspected, possibly superimposed on a background of an inherited neuropathy. Therefore, prolonged treatment trials with i.v. immunoglobulin i.v. methylprednisone, plasmapheresis, azathioprine, and i.v. cyclophosphamide were attempted, but produced no improvement in his neurological deficits.

Genetics Analysis

Genomic DNA was isolated from peripheral blood, and testing for PMP-22 deletion/duplication and point mutations, and *GJB-1* and *MPZ* mutations was negative. The 23 exons of *FIG4* were amplified by polymerase chain reaction and analyzed by automated sequencing in the University of Michigan Sequencing Core or as part of a diagnostic panel for patients with CMT at Athena Diagnostics (Worcester, MA). Analysis of individual gene sequence in the diagnostic panel was performed by PCR amplification of purified genomic DNA followed by automated bidirectional DNA sequencing of the entire coding region (23 exons for FIG4) including conserved flanking intronic sequences of the exon–intron splice junctions. Studies by Athena Diagnostics, Inc. (Marlborough, MA) indicate a 99% analytical sensitivity for mutations detection. Two heterozygous mutations in the *FIG4* gene consistent with CMT4J, the known p.I41T point mutation, and a novel intronic T > G transversion at IVS17-10, postulated to impair splicing. The p.I41T mutation is a known CMT4J-causing mutation whereas the T > G transversion at IVS17-10 had not been described previously and was not found in 0/380 control chromosomes tested by Athena Diagnostics.

Plasmids and Antibodies

AntiFIG4/Sac3 clone N202/7 was from UC Davis NeuroMab (Davis, CA), antiGAPDH from MediMabs (MM-0163-P, Montreal, QC, Canada), antiTRPV4 (ab63003), and antiLamp1 (ab25630) from Abcam (Cambridge, UK) and clone M2 antiflag from Sigma–Aldrich (Oakville, ON, Canada). Plasmid coding for enhanced green fluorescent protein (EGFP)-tagged pleckstrin homology domain of centaurin-b2

TABLE. Nerve Conduction Studies at Ages 36 and 43 Years

Motor Nerves		36 Years	Lat (ms)	Amp (mV)	CV (m/s)	43 Years	Lat (ms)	Amp (mV)	CV (m/s)
Left median	Wrist-APB		5.5	6.4			7.1	1.9	
	Elbow-wrist		15.5	3.7	25.4		15.9	NR	22
Left ulnar	Wrist-ADM		3.9	9.9			5.6	0.3	
	Be Elb-Wrist		16.5	3.9	18.9				
	Ab Elb-Be								
	Elb		21.5	2.5	21.2			NR	
Right tibial	Ankle-AHB		7.1	0.9			6	0.3	
	Knee-Ankle			NR				NR	
Left tibial	Ankle-AHB		6	1.1			NR		
	Knee-Ankle		45.8	1	10.1		NR		
Right peroneal	Ankle-EDB		10.2	0.1			NR		
	Knee-Ankle			NR			NR		
Sensory Nerves									
Right median	Wrist-digII		2.6	2.4	55.6		NR		
Left median	Wrist-digII		2.8	4	49.3		2.8	2.8	
Right ulnar	Wrist-digV		2.5	2	46.8		NR		
Left ulnar	Wrist-digV		2.4	4	50		3.3	1.5	
Right sural				NR			NR		
Right peroneal				NR			NR		

NR, no response; Lat, latency; Amp, amplitude, CV, conduction velocity.

binding specifically to PI(3,5)P_2 and EGFP-tagged pleckstrin homology domain of PIKfyve binding to PI(3)P were a gift from Dr. H.M. McBride (McGill University). pcDNA3.0-FLAG TRPV4 was a gift from Robert Lefkowitz (Addgene plasmid # 45751) and Dsred-TRPV4 was described previously (14). Plasmid used for *FIG4* knockout (KO) was Fig4CRISPR/Cas9 KO from Santa Cruz Biotechnology (Dallas, TX).

Fibroblast Cell Culture

Punch skin biopsies were obtained from the patient after informed consent, rinsed with PBS, minced into coarse slurry using iris scissors and transferred into a 15-mL plastic tube. The biopsy and consent forms were sent to the CellBank Repository for Mutant Cell Strains at Montreal Children's Hospital, McGill University Health Centre (Montreal, QC, Canada) for fibroblast culture and amplification. Control lines (MCH074 and MCH064) were provided from the CellBank repository of the Montreal Children's Hospital, McGill University Health Centre (Montreal, Canada) http://www.cellbank.mcgill.ca/ [last accessed 7 November 2014]. The fibroblasts were then immortalized as described previously (15). Lipofectamine 2000 and Optimem medium (Invitrogen, Carlsbad, CA) were used for transfection of immortalized fibroblasts according to the manufacturer's recommendation and grown in Dulbecco's Modified Eagle Medium with 10% FBS.

Primary Murine Spinal Cord Culture

Primary cultures of dissociated spinal cord-dorsal root ganglion were prepared and maintained in Eagle's Minimum Essential Media enriched with 5 g/L glucose and supplemented with 3% horse serum, and other growth factors as previously described and according to a protocol approved by the McGill University Animal Care Committee (16). Cultures were used in experiments 3–6 weeks following plating. Motor neurons in long-term primary spinal cord cultures are not transfectable, thus plasmids were expressed by intranuclear microinjection, which resulted in detection of the encoded protein by immunocytochemistry in at least 90% of injected cells after 48 hours. We used the CRISPR/CAS9 system in order to create a neuronal model of the disease by knocking out *FIG4* gene expression in 3-week-old cultured murine motor neurons using intranuclear injection of plasmids encoding Cas9, *FIG4* target sequences (or scramble) and EGFP to identify injected motor neurons. Under these conditions, significant downregulation of Fig4 expression occurred at day 2. Viability of motor neurons was assessed as in Bruening et al by counting daily the number of motor neurons expressing a marker of injected neurons, that is, EGFP encoded by pN1-EGFP in this study (17). Fibroblast motility was assessed over 24 hours by phase microscopy using an Olympus VivaView incubator microscope (Olympus, Richmond Hill, ON, Canada). Particular attention was paid to membrane ruffling, macropinocytopinosis and dynamics of endocytosis through observation of vacuoles emerging from the plasma membrane.

Fluorescence Recovery After Photobleaching (FRAP) and TRPV4 Dynamics

Fibroblasts expressing dsred-TRPV4 were grown in a matTek chamber (MatTek Corporation, Ashland, MA) for FRAP experiments using an inverted IX81 microscope coupled with the FV1000 confocal scanning microscope

(Olympus, Center Valley, PA), excited with the 565-nm laser. A Z-stack image of each fibroblast was taken before photobleaching to locate properly a region of interest (ROI) at the cell surface. Images were continuously recorded during the photo-bleaching step until the fluorescence intensity in the bleached ROI reached steady state (every second during 29 seconds). Image and data acquisition was performed using Metamorph (Universal Imaging, Sunnyvale, CA). Image reconstitution, particularly orthogonal reconstitution of the cells, and analysis were carried out using NIH Image J.

Statistics

Unpaired *t*-test was used for comparisons of means between 2 groups or 1-way ANOVA for >2 groups with a post hoc analysis by Tukey HSD test. Analyses were performed using Vassarstats software. Statistical significance was set at $p < 0.05$ and data were expressed as mean ± SD.

RESULTS

Cellular Phenotype

In immortalized fibroblasts derived from skin biopsy, FIG4 expression was strongly diminished, as shown by Western blot analysis (Fig. 1A), reminiscent of loss of function observed in other CMT4J cases, and consistent with the T > G transversion at IVS17-10, compatible with a splicing defect. Since no smaller molecular weight immunoreactive protein was detected, it is likely that the protein expressed by this allele is highly unstable. The remaining full-length protein expressed is expected to be derived from the p.I41T mutant allele.

Morphological analysis of patient's fibroblasts in comparison to control fibroblasts by phase microscopy demonstrated a typical FIG4 phenotype, that is, formation of larger vacuoles and an increase in the percentage of fibroblasts exhibiting this vacuolated phenotype (Fig. 1C, D). The distribution of lysosomes visualized by immunolabeling with antibody to LAMP1 was altered in 42% ± 5% of the patient's fibroblasts compared with 5% ± 3% in controls, $p < 0.05$ versus control, Student test (Fig. 1B) (2). The distribution of $PI(3,5)P_2$, which coats late endosomes and multivesiculate bodies, was detected by expressing a specific fluorescent probe (EGFP-tagged pleckstrin homology domain of centaurin-β2) (Fig. 2A) (18). The early endosomal marker PI(3)P was visualized by expressing plasmid encoding the specific fluorescent probe, EGFP-tagged 2XFYVE (Fig. 2B) (19). In the patient's fibroblasts, $PI(3,5)P_2$ and PI(3)P were dispersed throughout the cell body/cytoplasm whereas in control fibroblasts they were concentrated in the juxtanuclear regions suggesting impaired retrograde trafficking of multiple vesicular organelles (Figs. 1B, 2A, B). $PI(3,5)P_2$-coated structures appeared smaller as well as more dispersed in the patient's fibroblasts (Fig. 2A). Overall, disruption of inositol phosphate homeostasis by FIG4 mutations had a general effect on vesicular processing.

$PI(3,5)P_2$-Regulated Functions in FIG4-Deficient Fibroblasts

We further characterized the cellular phenotype of our patient's fibroblasts by demonstrating that 2 cellular processes regulated by $PI(3,5)P_2$ homeostasis (i.e. membrane ruffling and resistance to hyperosmotic shock) were affected. First, $PI(3,5)P_2$ is particularly involved in membrane ruffling and the last stages of macropinocytosis as it contributes to maturation and trafficking of late macropinosomes (20). Retrograde transport of vacuoles from the membrane ruffles was synchronous and involved waves of vacuoles in control fibroblasts, whereas retrograde transport of vacuoles was asynchronous and inefficient in the patient's fibroblasts as demonstrated by absence of waves of vacuoles emerging from the membrane ruffles (Fig. 3A). Retrograde transport of vacuoles from the membrane ruffles was synchronous and involved waves of vacuoles in 100% of control fibroblasts ($n = 3$, 60 cells per condition). Retrograde transport of vacuoles was asynchronous, as demonstrated by absence of waves of vacuoles emerging from the membrane ruffles (Fig. 3A), and inefficient in all (100%) patient's fibroblasts carrying the phenotypical feature shown in Figure 1C ($n = 3$, 51 cells per condition). This indicates that macropinocytosis and membrane remodeling is impaired when FIG4 is depleted.

Next, the effect of FIG4 deficiency on the response to hyperosmotic stress was investigated. Rapid changes in vacuolar volume and trafficking are tightly regulated during osmotic shock in order to maintain the vacuole membrane surface area constant and is part of the cellular adaptation to hyperosmotic stress (21). During hyperosmotic stress in yeast, the $PI(3,5)P_2$ level increases within the first 10 minutes and causes vesicles to become smaller and increase in number through fission (21, 22). To examine the effect of FIG4 deficiency on this process, control and patient's fibroblasts were treated with 0.4 M sorbitol to induce hyperosmotic shock. At 10 minutes after hyperosmotic shock, patient's fibroblasts remained resistant to adaptive shrinkage (Fig. 3B) and the number of large vacuoles increased (Fig. 3C). These data point to disruption of $PI(3,5)P_2$ homeostasis and function in the patient's fibroblasts.

TRPV4 Dynamics Are Affected by the Absence of FIG4

TRPV4 is an osmosensor cation channel that is mutated in CMT2C. Normally, this membrane protein is regulated by ubiquitinylation by beta arrestin and internalization of vesicles (23). Interestingly, inositol phosphates also modulate TRPV4 activity; for example, interaction of its ankyrin domain, which contains a cluster of CMT2C-causing mutations, and PI(4,5)P2 inhibits TRPV4 channel activity. On the other hand, IP(3)P sensitizes TRPV4 to osmo-transducing and mechano-transducing signals (12, 24). TRPV4 hyperactivation can indeed be toxic as shown by induction of cytotoxic hypercalcemia by hyperactive CMT2C-causing TRPV4 mutants in HeLa cells (13). Therefore, we hypothesized that since FIG4 affect inositol homeostasis and is important for endocytosis and retrograde transport of membrane components (7), TRPV4 trafficking and activity would be affected by FIG4 deficiency.

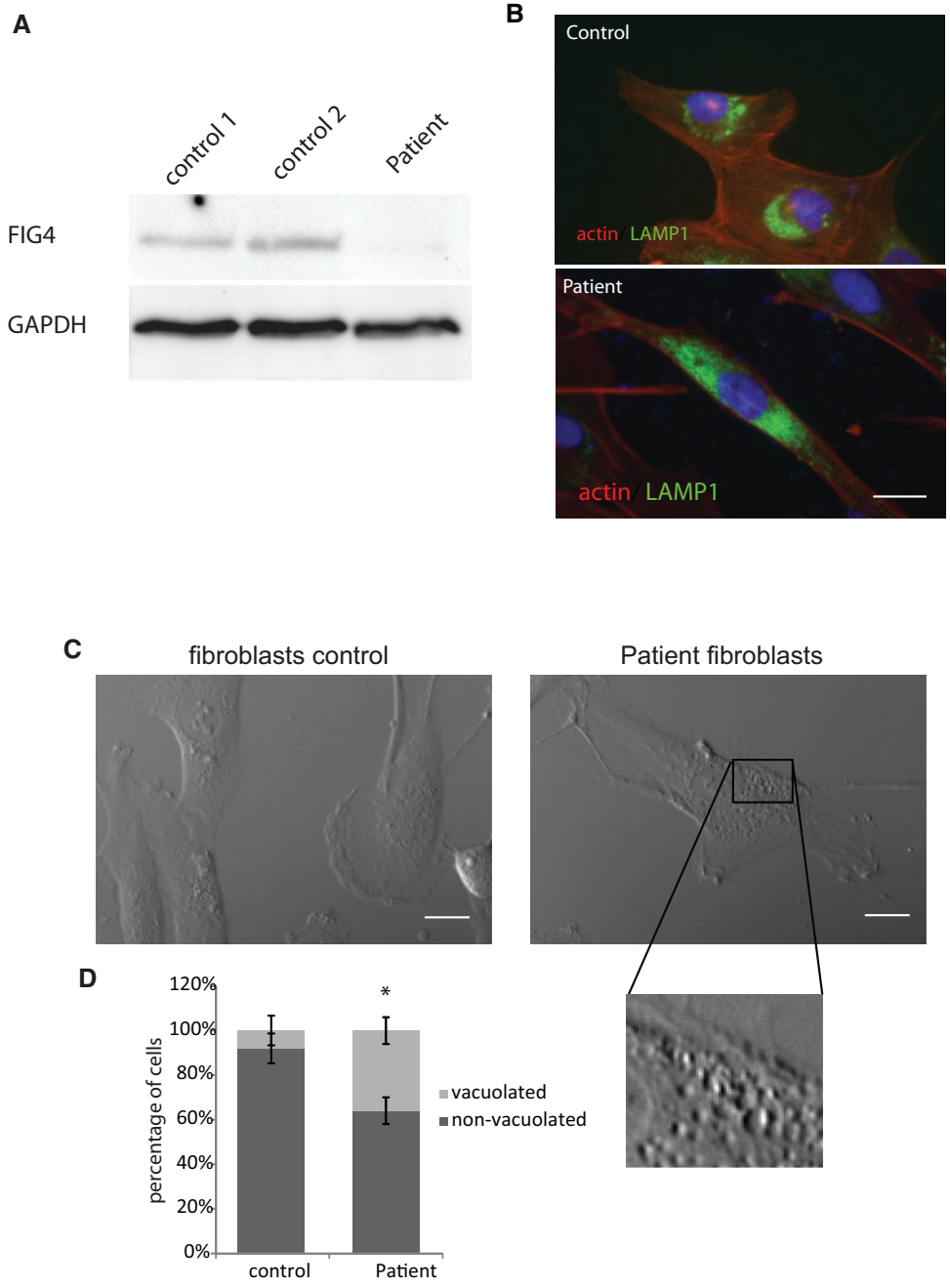

FIGURE 1. (A) Western blot analysis of FIG4 in immortalized fibroblasts of 2 control lines (control 1: MCH74 and control 2: MCH62) and our patient carrying FIG4 p.I41T point mutation and a novel intronic T > G transversion at IVS17-10. Downregulation of FIG4 expression in patient's fibroblasts was severe. **(B)** Immunolabeling of the lysosomal marker LAMP1 (green), actin (red), and DAPI (blue) in control (upper image) and patient fibroblasts (lower image) showing the much wider spread distribution of LAMP1 in the patient's fibroblasts. Scale bar: 10 μm. **(C)** Phase micrograph of control and patient's fibroblasts showing numerous vacuoles (insert) in the FIG4-deficient fibroblasts. Scale bar: 10 μm. **(D)** Increase in the percentage of cells with prominent cytoplasmic vacuoles in the patient fibroblast line ($n = 3$). *$p < 0.05$ Student *t*-test.

By Western blot analysis, TRPV4 levels (combined intensity of both bands normalized to GAPDH) were significantly increased in patient fibroblasts compared with control fibroblasts (mean ± SD: 1.48 ± 0.16 patient vs 0.81 ± 0.03, $n = 3$), representing a 182% increase in TRPV4 expression in FIG4 patient fibroblasts over control (Fig. 4A). By immunocytochemistry, TRPV4 labeling was mainly perinuclear and at the plasma membrane in control cells, whereas

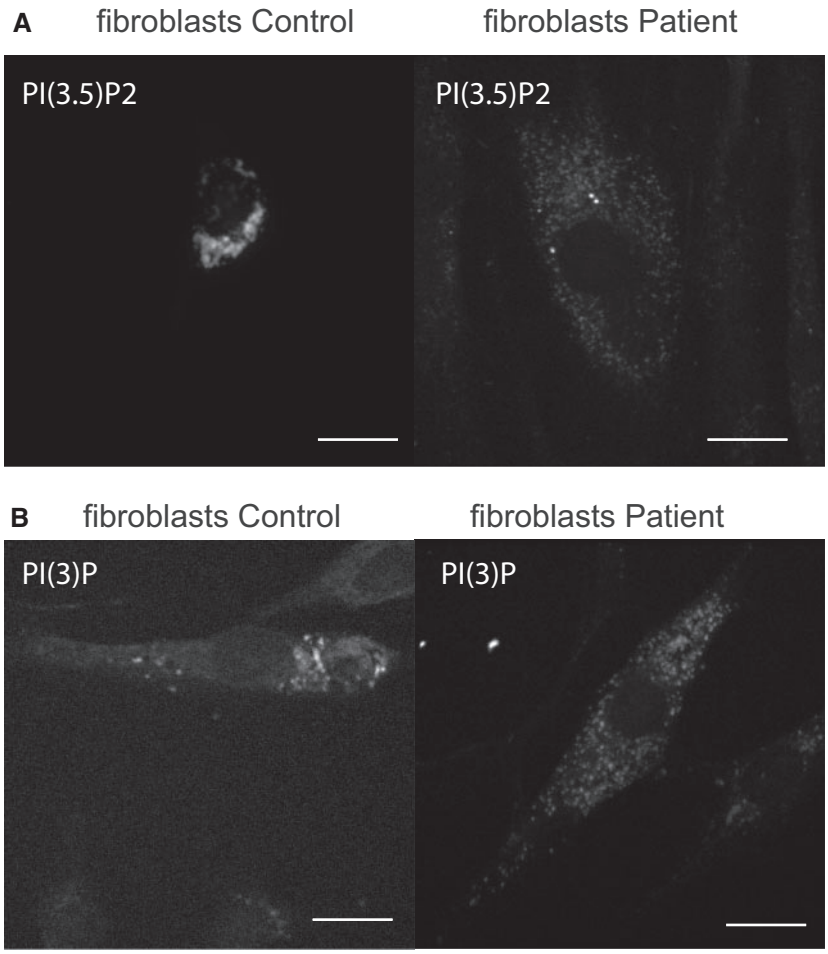

FIGURE 2. (A) PI(3,5)P_2 subcellular localization, assessed by expression of an EGFP-tagged pleckstrin homology domain of centaurin-β2 shows juxtanuclear concentration of PI(3,5)P_2 in control cells, but wide spread distribution in patient fibroblasts. Scale bar: 10 μm. Note that control image without PI(3,5)P expression is dark and show no signal. **(B)** PIP3 subcellular localization, assessed by expression of an EGFP-tagged 2XFYVE shows juxtanuclear concentration of PIP3 in control cells, but wide spread distribution in patient fibroblasts. Scale bar: 10 μm.

labeling was more abundant and widely distributed in the patient's fibroblast (Fig. 4B). To examine TRPV4 dynamics, TRPV4-dsred was expressed in fibroblasts. On 3D reconstructed confocal images, TRPV4 appeared more abundant at the plasma membrane of the patient's fibroblasts (Fig. 4C), suggesting interference with TRPV4 dynamics by FIG4 depletion. Cultures were immunolabeled with antibody to TRPV4 and the percentage of cells with TRPV4 localized at the plasma membrane was determined; 59% ± 6% of patient fibroblasts, but none of the control fibroblasts, exhibited this distribution (mean ± SD, examining 60 cells in each of 3 cultures; $p < 0.05$ patient *vs* control, Student test). TRPV4 mobility was assessed using confocal microscopy and FRAP of plasma membrane TRPV4. Recovery of TRPV4 fluorescence after focal photobleaching was delayed in patient's fibroblasts relative to controls, suggesting that mobility of TRPV4 was limited (Fig. 4D). Together the data suggest that FIG4 deficiency reduces TRPV4 trafficking, leading to overexpression at the plasma membrane and possibly hyperactivity.

TRPV4 Is Involved in Toxicity Induced by Fig4 Deficiency

We next assessed the toxicity of TRPV4 overexpression in cultured wild type motor neurons in long-term dissociated cultures of embryonic murine spinal cord, using techniques used in our laboratory to investigate ALS-causing mutant proteins (25). Overexpression of TRPV4 by plasmid microinjection was toxic, reducing motor neuron viability (Fig. 5).

In order to understand the role of TRPV4 in the FIG4 pathogenic cascade, experiments were carried out using the TRPV4-specific inhibitor, GSK2193874 (26). In addition to the fibroblast model, we developed a neuronal model of CMT4J by knocking out *Fig4* in cultured murine motor neurons (Fig. 6A) using the CRISPR/Cas9 system, reproducing features relevant to the disease, that is, cell death (Fig. 6B) and vacuolization (Fig. 6C). GSK213874 treatment significantly delayed death of $Fig4^{-/-}$ murine motor neurons (Fig. 6D), suggesting that TRPV4 hyperactivity contributes to the pathogenic cascade of Fig4-deficiency in motor neurons. Whereas GSK213874 inhibits TRPV4 activity, this treatment at 10 nM

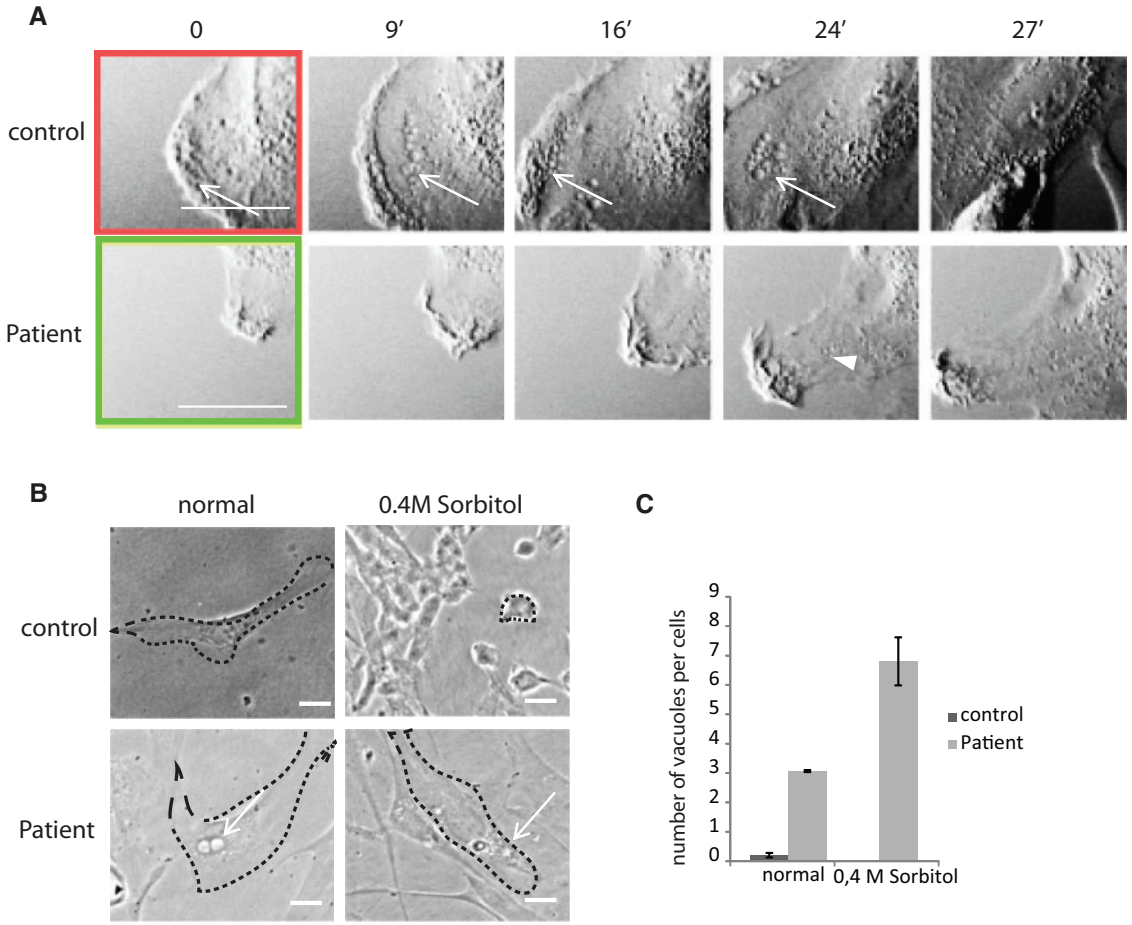

FIGURE 3. Time-lapse, phase contrast imaging of membrane ruffling and vacuolar trafficking in immortalized control and patient fibroblasts using the VivaView system. **(A)** Representative images (in minutes) of membrane ruffling showing synchronous and retrograde transport of vesicles (arrows) from the plasma membrane of control fibroblasts (upper panel) and patient's fibroblast (lower panel). Abnormal membrane ruffling in patient's fibroblasts was shown by poor progression of the membrane ruffling and rare retrogradely transported vacuoles emerging from the plasma membrane in patient fibroblasts (arrow head). Scale bar: 10 μm. **(B)** Phase micrographs of immortalized control or patient fibroblasts treated or not with 0.4 M sorbitol for 15 minutes as observed by phase microscopy. Patient's fibroblasts were resistant to cell shrinkage caused by hyperosmotic shock. Arrows show vacuoles. Scale bar: 10 μm. **(C)** A significant increase in the number of vacuoles per cell visible by phase-contrast in patient's fibroblasts relative to control fibroblasts after 15-minute treatment with 0.4M sorbitol ($n = 30$ cells per group), $^*p < 0.05$. 1 way ANOVA, Tukey's HSD post hoc analysis.

or 100 nM did not correct the abnormalities of vesicle formation and transport measured in patient's fibroblasts, suggesting that vacuolization is an upstream event (Supplementary Data Fig. S1).

DISCUSSION

Here, we describe a new intronic mutation of *FIG4* (T > G transversion at IVS17-10) found in compound homozygosity with the common p.I41T point mutation in a patient with a CMT4J phenotype. Biallelic polymorphism with compound heterozygous mutations FIG4(I41T/null) is typically found in CMT4J patients (3). The FIG4 mutations in our patient, p.I41T point mutation and the T > G transversion at IVS17-10, lead to a substantial decrease in FIG4 expression in skin biopsy-derived fibroblasts, consistent with the disease resulting from FIG4 deficiency, as in CMT4J patients with other heterozygous mutations. We did not observe any truncated form of FIG4, suggesting that, even if this intronic mutation still encodes a truncated mutant, this mutant is probably unstable. The small amount of full length protein would likely arise from the unstable $FIG4^{I41T}$ mutant and could provide some function. FIG4 is a $PI(3,5)P_2$ 5 phosphatase that is part of the Fab1 complex regulating the relative levels of PI(3)P and $PI(3,5)P_2$, phosphoinositols important for maturation and trafficking of endolysosomal vesicles. FIG4 not only has phosphatase activity, but also regulates the stability of the Fab1 complex; it is not clear which function is most important to CMT4J pathogenesis, but rescue of the neurodegenerative features in $Fig4^{-/-}$ mice by expressing a catalytic inactive FIG4 points to the importance of the integrity of the Fab1 complex in maintaining PI(3)P – $PI(3,5)P_2$ homeostasis (27).

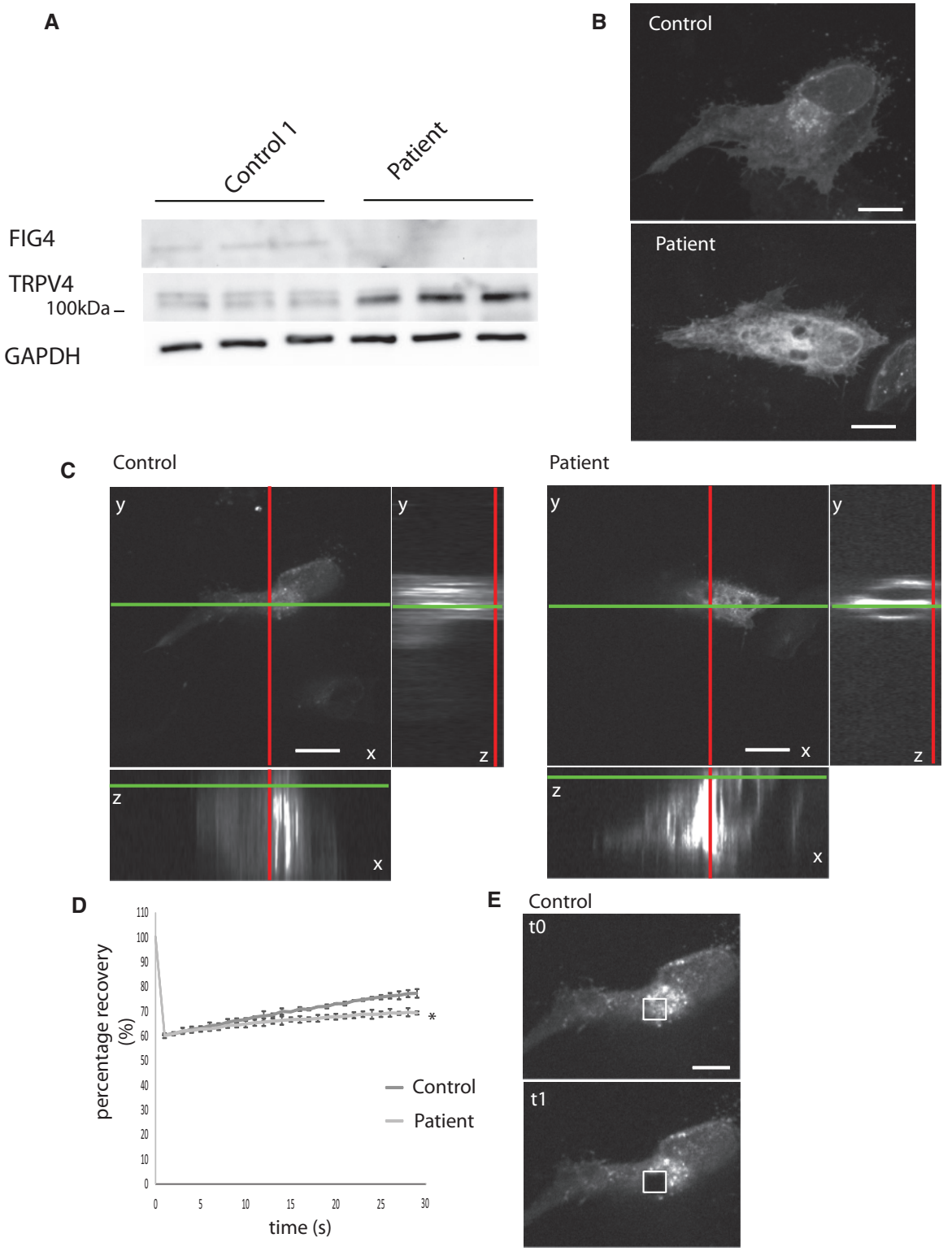

FIGURE 4. (A) Western blot analysis of 3 different protein extracts showing increased TRPV4 levels in patient's fibroblasts relative to the control line. GADPH was labeled as a loading control and FIG4 to identify patient cells. **(B)** Representative Z-stack reconstruction of confocal images of indirect immunofluorescence of endogenous TRPV4 in control and patient fibroblasts. Note the wide spread distribution of TRPV4 in patient fibroblasts. Scale bar: 10 μm. **(C)** Orthogonal view of Z-stacks of confocal images of a representative live control or patient fibroblast expressing dsRed-TRPV4 prior to performing FRAP. Z-positioning to the plasma membrane shows accumulation of TRPV4 at the plasma membrane in patient fibroblasts. Scale bar: 10 μm.

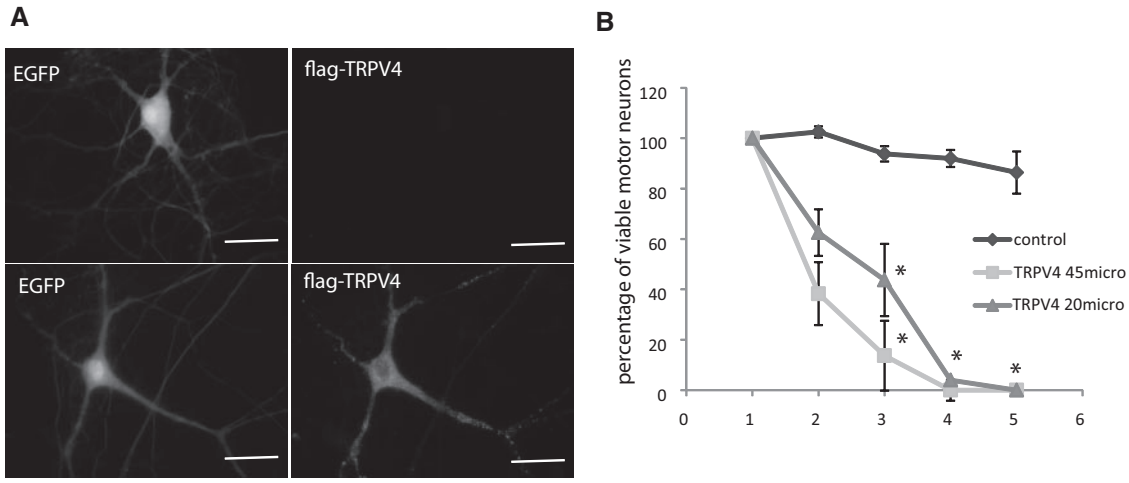

FIGURE 5. (A) Representative fluorescence image of cultured murine motor neurons ectopically expressing flag-TRPV4 following intranuclear microinjection of plasmids encoding flag-TRPV4 and EGPF at 20 μg/mL. Scale bar: 20 μm. **(B)** Viability of motor neurons expressing EGFP alone (control) or together with Flag-TRPV4 at 2 concentrations (20 or 45 μg/mL) over 5 days. Note the strong toxicity in motor neurons overexpressing TRPV4 at day 2. *$p < 0.05$ versus control *$p < 0.05$, Student test.

The data presented here point to abnormal transport and turnover of endocytic vesicles linked to disruption of phosphoinositol metabolism caused by FIG4 deficiency in our patient. Immortalized patient's fibroblasts showed increased presence of large vacuoles together with widespread dispersion of multiple vesicular organelles (lysosomes, early and late endosomes), rather than the normal juxtanuclear concentration. Retrograde trafficking of macropinocytic vesicles was impaired, consistent with abnormal endosomal trafficking underlying this abnormal distribution. Given the importance of vesicular trafficking in neuronal cells as a result of neurotransmission, the observations of PI(3)P and PI(3,5)P_2 using fluorescence probes showing that PI(3)P was more concentrated in the cell body, whereas PI(3,5)P_2 was highly abundant in dendrites as well as in the plasma membrane of the axon hillock demonstrate the importance of PI(3,5)P_2 in neurons (Supplementary Data Fig. S2).

Given the high load of vesicle recycling associated with neurotransmission, neurons would be expected to be highly vulnerable to PI(3,5)P_2 dysregulation. Indeed, PI(3,5)P_2 was highly abundant in cultured murine motor neurons, being distributed through the cell body and dendrites and at the axon hillock.

Phosphoinositols are also important for regulating activity of membrane ion channels, both directly in serving as ligands (e.g. PI(3,5)P_2 is the endogenous ligand of the lysosomal Ca^{2+} channel TRPML1 [9]) or indirectly through membrane internalization. The following data from this study implicate the transient receptor potential cation channel, TRPV4, in the pathogenesis of CMT4J: (1) The level of TRPV4 was increased in the patient's fibroblasts and FRAP studies indicated reduced turnover of TRPV4 at the plasma membrane. This increase in TRPV4 would be predicted to result in overall increase in cation conductance. (2) Overexpression of TRPV4 in cultured motor neurons was toxic. (3) Cell death induced by KO of Fig4 expression in cultured motor neurons was partially prevented by treatment with the TRPV4 inhibitor, GSK2193874. Membrane trafficking defects were not corrected by this treatment, but limiting ion conductance alone would be significant, given the high sensitivity of neurons to calcium toxicity (13).

Gain-of-function TRPV4 mutants also cause CMT2C characterized by increase in calcium influx to toxic levels (13). This increase in intracellular calcium was prevented by inhibiting TRPV4 calcium flux by ruthenium red in a HeLa cell model of CMT2C (13).

Although CMT2C and CMT4J are rare and patient descriptions scarce, these 2 forms have specific clinical features: Vocal cord paresis for CMT2C or nonuniform demyelination for CMT4J (28, 29). However, it is interesting to note that mutations in *FIG4* and *TRPV4* can both present as skeletal dysplasia and peripheral axonal neuropathy (1, 4, 30), which suggests common pathogenic mechanisms. We provide the proof of principle that TRPV4 inhibition could be a strategy for therapeutic development; however, further investigation will be necessary to demonstrate the efficiency of this strategy and the relative contribution of this pathway in CMT4J. The motor-predominant involvement with rapid progression of

FIGURE 4. Continued
(D) Recovery of dsRed-TRPV4 fluorescence after photobleaching of a region of interest at the plasma membrane in control or patient fibroblasts. The prebleach average fluorescence intensity of each image focused on the plasma membrane was set at 0, and the recovery is displayed as a percentage of fluorescence intensity relative to the prebleached region of interest (ROI), $n = 10$ for each condition. *$p < 0.05$ versus control, 1-way ANOVA, Tukey's HSD post hoc analysis. **(E)** Representative image of the surface of control fibroblast expressing dsRed-TRPV4 showing ROI before (upper panel) and after photo bleaching (lower panel). Scale bar: 10 μm.

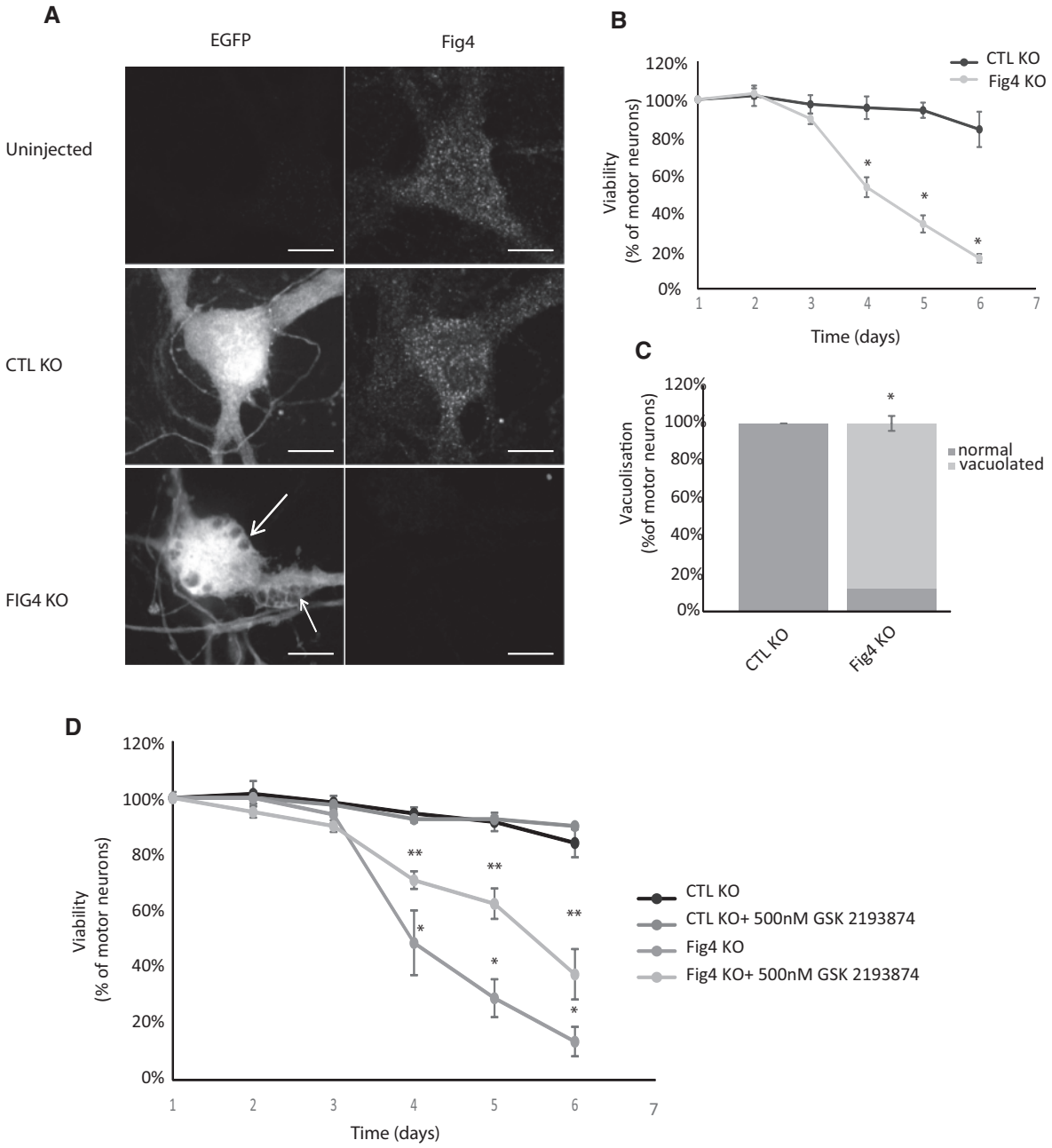

FIGURE 6. (A) Representative fluorescence images of Fig4 and EGFP in cultured murine motor neurons at day 3 postinjection of control (CTL) or *Fig4* knockout (KO) CRISPR/Cas9 plasmids (25 mg/mL). Down regulation of Fig4 was achieved in > 95% of motor neurons. Fig4 KO motor neurons show large vacuoles (arrows). Scale bar: 10 μm. **(B)** Daily viability of motor neurons expressing EGFP and Control KO CRISPR/Cas9 (CTL) or *Fig4* KO CRISPR/Cas9 (25 μg/mL). Loss of viability of *Fig4* KO motor neurons was significant at day 4. *$p < 0.05$ versus CTL KO 1-way ANOVA, Tukey's HSD post hoc analysis. **(C)** Increase in the percentage of motor neurons presenting vacuoles as shown in panel A at day 3 post injection of plasmids Control KO CRISPR/Cas9 (CTL KO) or *Fig4* KO CRISPR/Cas9 (25 μg/mL). *Fig4* KO toxicity in motor neurons starts at day 3. *$p < 0.05$ versus CTL. **(D)** Inhibiting TRPV4 significantly delayed loss of viability in *Fig4* KO motor neurons. Daily viability of motor neurons expressing EGFP and control KO CRISPR/Cas9 (CTL) or Fig4 KO CRISPR/Cas9 (25 μg/mL) with or without treatment with the TRPV4 inhibitor GSK2193874 at 500 nM beginning post injection for how long? *$p < 0.05$ *Fig4* KO versus CTL KO and **$p < 0.05$ *Fig4* KO versus *Fig4* KO+ GSK2193874 1-way ANOVA, Tukey's HSD post hoc analysis.

weakness and atrophy leading to complete quadriplegia in our patient is reminiscent of motor neuron diseases and we know that *FIG4* mutations can also present as ALS suggesting that TRPV4 may contribute to the pathophysiology of ALS (31). Indeed, overexpression of TRPV4 is observed in spinal cord motor neurons of $SOD1^{G93A}$ transgenic mice (32).

In conclusion, we have identified a new intronic mutation of FIG4 in a patient with severe CMT4J leading to loss of FIG4 expression and evidence that downstream upregulation of TRPV4 contributes to the pathogenic cascade of FIG4 loss-of-function. These findings point to a functional overlap between CMT4J and CMT2C due to gain-of-function mutations in TRPV4.

ACKNOWLEDGEMENTS

We thank Sandra Minotti for technical assistance with cell culture, Dr. Heidi M. McBride for her generous gift of the plasmids and Dr. Eric A. Shoubridge for assistance in fibroblast culture and immortalization.

REFERENCES

1. Bird TD, Charcot–Marie–Tooth hereditary neuropathy overview. In: Pagon RA, Adam MP, Ardinger HH, et al. eds. GeneReviews® [Interner]. NCBI bookshelf. Bookshelf ID: NBK138600 Seattle, WA 1993–2017.
2. Chow CY, Zhang Y, Dowling JJ, et al. Mutation of FIG4 causes neurodegeneration in the pale tremor mouse and patients with CMT4J. Nature 2007;448:68–72
3. Nicholson G, Lenk GM, Reddel SW, et al. Distinctive genetic and clinical features of CMT4J: a severe neuropathy caused by mutations in the PI(3,5)P(2) phosphatase FIG4. Brain 2011;134:1959–71
4. Campeau PM, Lenk GM, Lu JT, et al. Yunis-Varon syndrome is caused by mutations in FIG4, encoding a phosphoinositide phosphatase. Am J Hum Genet 2013;92:781–91
5. Zhang X, Chow CY, Sahenk Z, et al. Mutation of FIG4 causes a rapidly progressive, asymmetric neuronal degeneration. Brain 2008;131: 1990–2001
6. Guo J, Ma YH, Yan Q, et al. Fig4 expression in the rodent nervous system and its potential role in preventing abnormal lysosomal accumulation. J Neuropathol Exp Neurol 2012;71:28–39
7. Sbrissa D, Ikonomov OC, Fu Z, et al. Core protein machinery for mammalian phosphatidylinositol 3,5-bisphosphate synthesis and turnover that regulates the progression of endosomal transport. Novel Sac phosphatase joins the ArPIKfyve–PIKfyve complex. J Biol Chem 2007;282: 23878–91
8. Nicot AS, Laporte J. Endosomal phosphoinositides and human diseases. Traffic 2008;9:1240–9
9. Zou J, Hu B, Arpag S, et al. Reactivation of lysosomal Ca^{2+} efflux rescues abnormal lysosomal storage in FIG4-deficient cells. J Neurosci 2015;35:6801–12
10. Strotmann R, Harteneck C, Nunnenmacher K, et al. OTRPC4, a nonselective cation channel that confers sensitivity to extracellular osmolarity. Nat Cell Biol 2000;2:695–702
11. Garcia-Elias A, Lorenzo IM, Vicente R, et al. IP3 receptor binds to and sensitizes TRPV4 channel to osmotic stimuli via a calmodulin-binding site. J Biol Chem 2008;283:31284–8
12. Takahashi N, Hamada-Nakahara S, Itoh Y, et al. TRPV4 channel activity is modulated by direct interaction of the ankyrin domain to PI(4,5)P(2). Nat Commun 2014;5:4994
13. Klein CJ, Shi Y, Fecto F, et al. TRPV4 mutations and cytotoxic hypercalcemia in axonal Charcot–Marie–Tooth neuropathies. Neurology 2011; 76:887–94
14. Sonkusare SK, Dalsgaard T, Bonev AD, et al. AKAP150-dependent cooperative TRPV4 channel gating is central to endothelium-dependent vasodilation and is disrupted in hypertension. Sci Signal 2014;7:ra66
15. Yao J, Shoubridge EA. Expression and functional analysis of SURF1 in Leigh syndrome patients with cytochrome c oxidase deficiency. Hum Mol Genet 1999;8:2541–9
16. Roy J, Minotti S, Dong L, et al. Glutamate potentiates the toxicity of mutant Cu/Zn-superoxide dismutase in motor neurons by postsynaptic calcium-dependent mechanisms. J Neurosci 1998;18:9673–84
17. Bruening W, Roy J, Giasson B, et al. Up-regulation of protein chaperones preserves viability of cells expressing toxic Cu/Zn-superoxide dismutase mutants associated with amyotrophic lateral sclerosis. J Neurochem 1999;72:693–9
18. Dowler S, Currie RA, Campbell DG, et al. Identification of pleckstrin-homology-domain-containing proteins with novel phosphoinositide-binding specificities. Biochem J 2000;351:19–31
19. Gillooly DJ, Morrow IC, Lindsay M, et al. Localization of phosphatidylinositol 3-phosphate in yeast and mammalian cells. EMBO J 2000;19: 4577–88
20. Ho CY, Alghamdi TA, Botelho RJ. Phosphatidylinositol-3,5-bisphosphate: no longer the poor PIP2. Traffic 2012;13:1–8
21. Dove SK, Cooke FT, Douglas MR, et al. Osmotic stress activates phosphatidylinositol-3,5-bisphosphate synthesis. Nature 1997;390: 187–92
22. Duex JE, Nau JJ, Kauffman EJ, et al. Phosphoinositide 5-phosphatase Fig 4p is required for both acute rise and subsequent fall in stress-induced phosphatidylinositol 3,5-bisphosphate levels. Eukaryot Cell 2006;5:723–31
23. Shukla AK, Kim J, Ahn S, et al. Arresting a transient receptor potential (TRP) channel: beta-arrestin 1 mediates ubiquitination and functional down-regulation of TRPV4. J Biol Chem 2010;285:30115–25
24. Fernandes J, Lorenzo IM, Andrade YN, et al. IP3 sensitizes TRPV4 channel to the mechano- and osmotransducing messenger 5′-6′-epoxyeicosatrienoic acid. J Cell Biol 2008;181:143–55
25. Durham HD, Roy J, Dong L, et al. Aggregation of mutant Cu/Zn superoxide dismutase proteins in a culture model of ALS. J Neuropathol Exp Neurol 1997;56:523–30
26. Thorneloe KS, Cheung M, Bao W, et al. An orally active TRPV4 channel blocker prevents and resolves pulmonary edema induced by heart failure. Sci Transl Med 2012;4:159ra48
27. Lenk GM, Frei CM, Miller AC, et al. Rescue of neurodegeneration in the Fig4 null mouse by a catalytically inactive FIG4 transgene. Hum Mol Genet 2016;25:340–7
28. Chen DH, Sul Y, Weiss M, et al. CMT2C with vocal cord paresis associated with short stature and mutations in the TRPV4 gene. Neurology 2010;75:1968–75
29. Cottenie E, Menezes MP, Rossor AM, et al. Rapidly progressive asymmetrical weakness in Charcot–Marie–Tooth disease type 4J resembles chronic inflammatory demyelinating polyneuropathy. Neuromuscul Disord 2013;23:399–403
30. White JP, Cibelli M, Urban L, et al. TRPV4: molecular conductor of a diverse orchestra. Physiol Rev 2016;96:911–73
31. Chow CY, Landers JE, Bergren SK, et al. Deleterious variants of FIG4, a phosphoinositide phosphatase, in patients with ALS. Am J Hum Genet 2009;84:85–8
32. Lee JC, Joo KM, Choe SY, et al. Region-specific changes in the immunoreactivity of TRPV4 expression in the central nervous system of SOD1(G93A) transgenic mice as an in vivo model of amyotrophic lateral sclerosis. J Mol Histol 2012;43:625–31